

# Gyrodometry: A New Method for Combining Data from Gyros and Odometry in Mobile Robots

by  
J. Borenstein and L. Feng  
The University of Michigan

Advanced Technologies Lab, 1101 Beal Ave.  
Ann Arbor, MI 48109-2110  
Email: johannb@umich.edu and Feng@engin.umich.edu

## ABSTRACT

This paper presents a very simple, yet very effective method for combining measurements from a gyro with measurements from wheel encoders (odometry). Sensor-fusion of this kind has been done before, usually by means of a statistical model that describes the behavior of the gyro and the behavior of the odometry component. However, because these systems are based on models, they cannot anticipate the unpredictable and potentially "catastrophic" effect of larger bumps or objects occasionally encountered on the floor.

By contrast, our method, called Gyrodometry, has been developed based on a careful study of the physical interaction between the ground and the vehicle. We present experimental evidence that non-systematic odometry error sources (such as bumps) impact the vehicle only during very short periods; typically a fraction of a second for each encounter. During these short instances the readings from the gyro and from odometry differ significantly, while in the absence of large non-systematic errors the readings are very similar. Gyrodometry makes use of this observation by using odometry data only — most of the time, while substituting gyro data only during those brief instances during which gyro and odometry data differ substantially. This way the ill-effects of gyro drift are almost completely eliminated, and our method can thus make use of inexpensive gyros with large drift rates. Experimental data is presented that demonstrates the effectiveness of this approach.

## 1. INTRODUCTION AND BACKGROUND

In most mobile robot applications two basic position-estimation methods are employed together: absolute and relative positioning [Byrne et al., 1992; Chenavier and Crowley, 1992; Evans, 1994]. Absolute positioning methods usually rely on navigation beacons, active or passive landmarks, map matching, or satellite-based navigation signals. Each of these absolute positioning approaches can be implemented by a variety of methods and sensors. Yet, none of the currently existing systems is particularly elegant, and usually these systems are somewhat expensive. A comprehensive survey on mobile robot positioning methods is given in [Borenstein et al., 1995].

Relative positioning is usually based on odometry. Odometry is simple, inexpensive, and easy to accomplish in real-time. The disadvantage of odometry is its unbounded accumulation of errors.

With the introduction of optical fiber gyros the use of gyros has become more attractive for mobile robot applications. However, gyros have relatively large drift rates, which cause unbounded growth in orientation errors.

Because of their potential for unbounded growth of errors, odometry and gyros can only be used in conjunction with periodic absolute position updates. Nonetheless, improving odometry and gyro accuracy helps increase the travel distance in-between absolute position updates, and thus results in lower installation and operating costs for the whole system.

## 1.1 Properties of odometry errors

In this section we discuss properties of odometry as they relate to differential-drive vehicles (i.e., vehicles that have two independently driven wheels). Optical encoders are typically mounted on the drive motors to count the wheel revolutions. Using simple geometric equations, it is straight-forward to compute the momentary position of the vehicle relative to a known starting position. This computation is called odometry. It is important to note that when considering errors in odometry, orientation errors are the main source of concern. This is so because once incurred, orientation errors grow without bound into lateral position errors [Feng et al., 1993].

Odometry is based on the assumption that wheel revolutions can be translated into linear displacement relative to the floor. This assumption is only of limited validity. One extreme example is wheel slippage: if one wheel was to slip on, say, an oil spill, then the associated encoder would register wheel revolutions even though these revolutions would not correspond to a linear displacement of the wheel.

Besides this extreme case of total slippage, there are several other, more subtle reasons for inaccuracies in the translation of wheel encoder readings into linear motion. All of these error sources fit into one of two categories: (1) systematic errors and (2) non-systematic errors.

### 1. Systematic errors

- a. Unequal wheel diameters
- b. Average of both wheel diameters differs from nominal diameter
- c. Misalignment of wheels
- d. Uncertainty about the effective wheelbase (due to non-point wheel contact with the floor)
- e. Limited encoder resolution
- f. Limited encoder sampling rate

### 2. Non-systematic errors

- a. Travel over uneven floors
- b. Travel over unexpected objects on the floor
- c. Wheel-slippage

In recent work we introduced "UMBmark," a method for measuring and correcting systematic odometry errors in differential-drive mobile robots [Borenstein and Feng, 1995a; 1995b]. With this method we were able to reduce the systematic odometry error of an uncalibrated LabMate robot [TRC] by one order of magnitude. However, this measure alone cannot guarantee trouble-free odometry, because occa-

sional bumps, cracks or other large disturbances can cause unpredictable "catastrophic" odometry errors that can easily lead to the complete failure of the robot's mission. The method presented in this paper is designed to detect and correct such "catastrophic" non-systematic odometry errors.

## 1.2 The use of gyros in mobile robot applications

An extensive study of the use of gyroscopes in mobile robots was conducted by [Barshan and Durrant-Whyte, 1995]. One of the tested instruments was the ENV-O5S Gyrostar from [MURATA] and the other was the Solid State Angular Rate Transducer (START) gyroscope manufactured by [GEC]. Barshan and Durrant-Whyte evaluated the performance of these two gyros and found that they suffered relatively large drift, on the order of 5 to 15°/min. The Oxford researchers then developed a sophisticated error model for the gyros, which was subsequently used in an Extended Kalman Filter (EKF). At the end of a 5-minute experiment, the START had accumulated a heading error of -70.8° while the error of the Gyrostar was -59°. With the EKF, the accumulated errors were much smaller: 12° was the maximum heading error for the START gyro, while that of the Gyrostar was -3.8°. Overall, the results from applying the EKF show a 5 to 6-fold reduction in the angular measurement after a five-minute test period. However, even with the EKF, a drift rate of 1 to 3°/min can still be expected.

Komoriya and Oyama [1994] conducted a study of a system that used the OFG-3 [HITACHI] optical fiber gyroscope in conjunction with odometry information. This fusion of information from these two different sensor systems was realized through a Kalman Filter. Komoriya and Oyama tested their method in actual experiments with a mobile robot. In one set of experiments their robot was instructed to follow a triangular path of 5 m total length. The robot's maximum speed was 0.14 m/s and that speed was further reduced at the corners of the path. The results of this experiment indicate an average position error of about 5 mm. However, it is not immediately evident how this error was found. We interpret the quoted results as showing a position error that was computed by the onboard computer, but not measured absolutely.

In both of the above studies a Kalman Filter approach was taken to reduce the drift and to fuse odometry and gyro data. Kalman filters require a detailed model of the sensors and the interaction between the wheels and the floor (i.e., odometry). To model

odometry researchers typically define "error ellipsis" that describe the probability of the robot to be indeed at the location its odometry has determined. These models are usually based on the robot's systematic errors, but they cannot take into account non-systematic errors and especially "catastrophic" events like the encounter of a bump, crack, or other irregularity of the floor.

To overcome this problem, we took a different approach. We studied the physical interaction between the floor and the wheels during "catastrophic" events. We present relevant results of this study in Section 2. Based on these results we developed Gyrodometry, a method for improving odometric accuracy with gyros regardless of the gyro's drift rate (see Section 3). Section 4 presents initial experimental results from implementing Gyrodometry on a LabMate robot.

In the experiments described in the following sections we used the Murata Gyrostar [Murata] model ENV-05H (see Fig. 1). The Gyrostar is a piezoelectric vibrating gyroscope with analog voltage output that varies linearly with the measured rate of rotation. connection to a computer. The drift rate we measured in practice was 3 to 15°/min (similar to the drift observed by [Barshan and Durrant-Whyte, 1995] for their Gyrostar sensor). We will assume an average drift rate of 10°/min = 0.166°/s. A detailed discussion of gyroscopes for mobile robot applications is given in [Borenstein et al., 1996].



Figure 1: The Murata Gyrostar ENV-05H was used in the experiments in this paper.

## 2. ANALYSIS

When the left wheel ( $W_L$ ) of a differential-drive robot like the LabMate travels over a bump (or crack, or other irregularity), then  $W_L$ 's total travel distance would have to increase by an amount  $\Delta D$  if the robot was to maintain straight-line motion.  $\Delta D$  is a function of the wheel diameter and the height of the bump (see [Borenstein, 1995] for a detailed analysis). However, for straight-line motion the low-level controller of a conventional differential-drive mobile robot will try to keep the rotational velocities of both wheels equal. Thus, the horizontal distance traveled by  $W_L$  will be  $\Delta D$  less than that of  $W_R$ , causing a curved motion into the direction of the bump. After traversing the bump, the vehicle will continue in straight-line motion, but with a constant orientation error  $\Delta\theta_{\text{bump}}$ , given by  $\Delta\theta_{\text{bump}} \approx \Delta D/b$ , where  $b$  is the wheelbase of the robot.

One further effect that is noticeable while traversing a bump is that the vehicle will first turn toward the bump, then away from it. This is so because the wheel that encounters the bump ( $W_L$ ) slows down momentarily as some of the kinetic energy from the forward motion is converted into potential energy associated with the higher elevation of the vehicle on top of the bump. Then, when the robot rolls off the bump, it regains its velocity and turns back (almost) to its original orientation. The wheel encoders are aware of the change in velocity and will provide correct data on the event. However, the wheel encoders are not aware that  $W_L$  traveled the extra distance  $\Delta D$ . Because of this, the robot does not turn back completely in the original direction of motion, thereby establishing the constant orientation error  $\Delta\theta_{\text{bump}}$  described above.

Figure 2 provides experimental data in support of the above model. In the experiment of Fig. 2 a LabMate robot traveled at a slow speed of 10 cm/s on a smooth concrete floor. The custom-built motor controller that we installed on that vehicle uses a so-called cross-coupling control algorithm [Feng et al., 1993] that tries to maintain equal encoder pulses from both wheels at all times. The vehicle ran for 140 s ( $\approx 14$  m) and artificial bumps (see Table I) were introduced by placing pieces of different-diameter household extension cables under the right wheel at roughly 1-m intervals.

The momentary orientation of the vehicle based on odometry is plotted and labeled  $\theta_{\text{odo}}$  in Fig. 2. Since the odometry computation is unaware of the error  $D$ , the bumps cause only a short swerve for each encounter, but the vehicle returns to its original orientation (at least, that's what the odometry algorithm "thinks").

The momentary orientation of the robot as measured with the Gyrostar is plotted and labeled gyro in Fig. 2. The magnitude of the swerve as measured by the gyro is similar to that measured by odometry. However, the gyro-plot shows that after each swerve there is a clearly discernible residual increment in the orientation of the vehicle, on the order of  $0.5^\circ$  -  $0.8^\circ$  for the larger bumps.

Since the odometry computation is unaware of the error  $\Delta D$ , the bumps cause only a short swerve for each encounter, but the vehicle returns to its original orientation (at least, that's what the odometry algorithm "thinks").

The momentary orientation of the robot as measured with the Gyrostar is plotted and labeled  $\theta_{\text{gyro}}$  in Fig. 2.

While Fig. 2 explains some of the physical aspects of the robot's encounter with bumps, the figure does not provide information on the accuracy of the gyro data. For example, we cannot tell the actual drift of the gyro from examining Fig. 2. An absolute measure of the robot's momentary orientation is needed, against which the gyro-data can be plotted. To obtain such an absolute measure we installed a simple wall-following system, based on two sideways facing Polaroid ultrasonic sensors. Then, when traveling along a continuous, straight wall, it is possible to measure the absolute orientation of the robot to within typically  $\pm 0.25^\circ$ . The momentary orientation of the robot, according to the sonar wall-following sensor, is shown and labeled  $\theta_{\text{sonar}}$  in Fig. 2. According to the sonars, at the end of this run the accumulated orientation error is  $\sim 9^\circ$ . One can also see now that the gyro readings were off by approximately  $4.2^\circ$  at the end of the run. We attribute this discrepancy to the drift rate of the gyro; here about  $4.2^\circ/140 \text{ s} = 0.03^\circ/\text{s} = 1.8^\circ/\text{min}$ .

The effect of a single bump on the robot's sensors is shown in Fig. 3. The plot shows the change in ori-

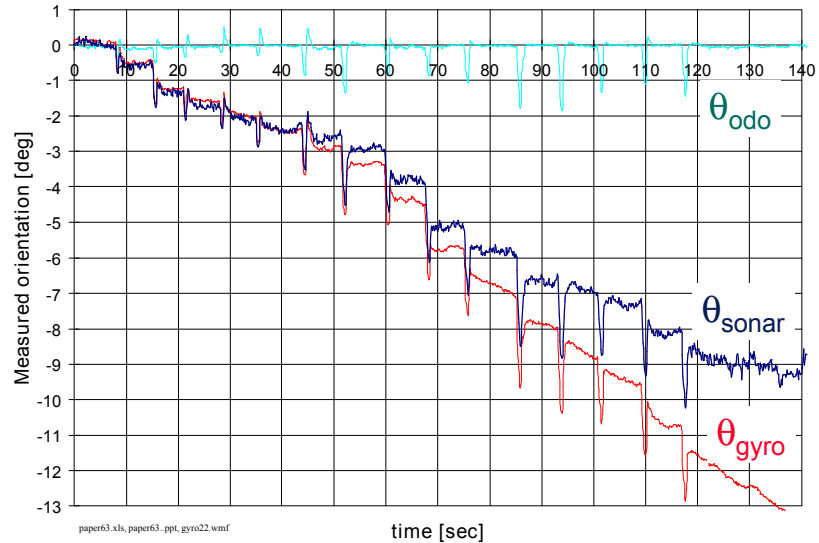


Figure 2: Momentary orientation of the robot as measured by odometry ( $\theta_{\text{odo}}$ ), the Gyrostar ( $\theta_{\text{gyro}}$ ), and the "completely accurate" wall-following sonars ( $\theta_{\text{sonar}}$ ). During this 2:20-minute run at 10 cm/s, the robot encountered 15 bumps of different heights under its right wheel.

entation of the robot per sampling interval, as measured by odometry ( $\Delta\theta_{\text{odo}}$ ) and by the gyro ( $\Delta\theta_{\text{gyro}}$ ). The experiment is similar to that of Fig. 2, except that the data for Fig. 3 came from an earlier test with a different gyro and a single bump was encountered by the left wheel, at  $t = 73 \text{ s}$ . The sampling interval in this experiment was  $T = 0.1 \text{ s}$ .

Figure 3 shows how the vehicle first turns toward the bump (ccw, positive portion of the curve) while the affected wheel climbs up the bump, then away from the bump (cw), while the affected wheel rolls off the bump. Since the robot controller is set up to maintain equal encoder pulse counts, the robot steers back to its "original" direction after traversing the bump. However, since odometry missed some of the initial turning, the robot does not completely turn back to its original orientation and thus retains a large residual orientation error.

We interpret the gyro-measured change of orientation,  $\Delta\theta_{\text{gyro}}$ , as an almost accurate representation of the actual rotation performed by the vehicle. We do so because the typical drift rate of the Gyrostar ( $0.03^\circ/\text{s}$ ) is negligible when compared to the peak rate of rotation, which is reached at  $t = 72.9 \text{ s}$  and which amounts to  $0.7^\circ/0.1 \text{ s} = 7^\circ/\text{s}$ . Based on these values, the drift rate of the Gyrostar (we assumed an average drift of  $0.166^\circ/\text{s}$  in Section 1) introduces an acceptable inaccuracy of  $0.166/7 \approx 2.37\%$  compared to the peak rate.

Table 1: Objects used to create the bumps in Fig. 2

Bumps 1-5	Bumps 6-10	Bumps 11-15
6-mm dia. cable	9-mm dia. Cable	12-mm dia cable

### 3. GYRODOMETRY

In this section we introduce Gyrodometry — a new method for fusing data from a gyro with data obtained from odometry. As we explained in Section 1, one of the most serious problems with odometry is the potential for "catastrophic" non-systematic errors, such as those caused by bumps or other large irregularities on the ground. We also argued that the robot cannot be calibrated to compensate for non-systematic errors, nor that it is possible to predict the frequency or magnitude of these errors. Similarly, we recalled that the foremost problem with gyros is their inherent drift, which results in continuous and unbounded growth of the orientation error. Gyrodometry reduces the ill-effects of these problems.

The Gyrodometry method is based on the hypothesis that the discrepancy between the odometry curve and the gyro curve persists only over a very short amount of time. The experimental data in Fig. 3 lends credence to this hypothesis, as can be seen by investigating the line labeled  $\Delta\theta_{\text{gyro}} - \Delta\theta_{\text{odo}}$  in Fig. 3. This line shows the difference between the odometry and the gyro measurements, defined as

$$\Delta_{G-O} = \Delta\theta_{\text{gyro}} - \Delta\theta_{\text{odo}}.$$

The Gyrodometry method now simply compares  $\Delta_{G-O}$  to a preset threshold, for example

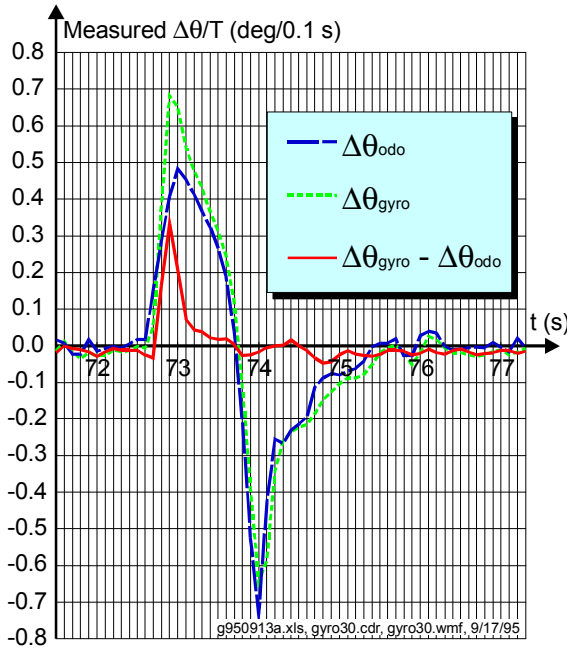


Figure 3: Effect of a single bump on the vehicle's change of orientation per sampling interval, as measured by odometry and by the gyro. The bump was a 9-mm dia. cable placed under the left wheel.

$\Delta\theta_{\text{thres}} = 0.125^\circ/T$ . Then, if  $|\Delta_{G-O}| > \Delta\theta_{\text{thres}}$ , the robot's momentary orientation  $\theta_i$  is computed based on  $\Delta\theta_{\text{gyro}}$ ; if  $|\Delta_{G-O}| < \Delta\theta_{\text{thres}}$ , then  $\theta_i$  is computed based on  $\Delta\theta_{\text{odo}}$ . The complete implementation of the Gyrodometry method can thus be expressed by this simple pseudo-code statement:

```

if ( $|\Delta_{G-O,i}| > \Delta\theta_{\text{thres}}$ )
then  $\theta_i = \theta_{i-1} + \Delta\theta_{\text{gyro},i} T$ 
else  $\theta_i = \theta_{i-1} + \Delta\theta_{\text{odo},i} T$ 

```

One can see in Fig. 3 that  $|\Delta_{G-O}| > \Delta\theta_{\text{thres}}$  is true for only three sampling intervals ( $=0.3$  s). Yet, this short amount of time accounts for most of the difference between  $\theta_{\text{gyro}}$  and  $\theta_{\text{odo}}$ . Consequently, the robot's dead-reckoning systems relies on the gyro data only for a small fraction of the total travel time, keeping the system largely free of the drift associated with the gyroscope. On the other hand, the gyro data covers those intervals in which the odometry error would have been largest. The effectiveness of the Gyrodometry method is illustrated by experimental results presented in the next section.

In this section we present experimental results that illustrate the effectiveness of the Gyrodometry method. For the sake of consistency, we have used the same set of experimental data that was used in Figure 2 for Figure 4 in this section. One should note, though, that we have actually conducted many experimental runs — all with similarly good results as those shown here.

Before we present the experimental results we have to define the following orientation errors (recall that we consider the sonar-based orientation measurements as "completely correct").

$$\epsilon_{\text{odo}} = \theta_{\text{odo}} - \theta_{\text{sonar}} \quad (2a)$$

$$\epsilon_{\text{gyro}} = \theta_{\text{gyro}} - \theta_{\text{sonar}} \quad (2b)$$

$$\epsilon_{\text{go}} = \theta_{\text{go}} - \theta_{\text{sonar}} \quad (2c)$$

where

$\theta_{\text{odo}}$ ,  $\theta_{\text{gyro}}$ ,  $\theta_{\text{sonar}}$ ,  $\theta_{\text{go}}$  — Momentary orientation as computed by odometry, the gyro, the sonars, and the Gyrodometry method, respectively.

$\epsilon_{\text{odo}}$ ,  $\epsilon_{\text{gyro}}$ ,  $\epsilon_{\text{go}}$  — Momentary orientation error as computed by odometry, the gyro, and the Gyrodometry method, respectively.

Although the experimental data used in Fig. 4 is identical to the data used for Fig. 2, Fig. 4 differs in that it shows a plot of the orientation errors  $\epsilon_{\text{odo}}$ ,  $\epsilon_{\text{gyro}}$ , and  $\epsilon_{\text{go}}$  as defined above. Interestingly, it appears that

the Gyrodometry error  $\epsilon_{go}$  does not increase with either the odometry-only error nor with the gyro-only drift. The maximal error  $\epsilon_{go}$  (during normal travel, i.e., not during a transient) stayed well under  $\pm 0.5^\circ$ . Thus the Gyrodometry error was about 18 times smaller than the odometry-only error and about eight times smaller than the gyro-only error at the end of the experiment ( $-4^\circ$ ). It is also evident from Fig. 4 that had we continued the experiment further, the performance of the Gyrodometry method relative to the gyro would have increased further. However, the length of travel was limited to the length of the largest uninterrupted wall we could find in our laboratory, for using the sonar wall-following sensor. Running at a lower speed than 10 cm/s is unfeasible with the LabMate robot.

## 5. CONCLUSIONS

This paper introduces a new method for combining data from gyros and from odometry. This method, called Gyrodometry, is exceedingly easy to implement, yet it appears to be very effective in reducing odometry errors due to non-systematic "catastrophic" errors such as those caused by bumps or other large irregularities on the floor.

Although our current set of experiments covers only straight line motion, we are optimistic that the method can be extended easily to turning motion as well. This is so because the Gyrodometry method acts upon the difference between momentary odometry and gyro readings. This difference should behave similarly during turning and straight-line motion. We will investigate this matter in the immediate future.

### Acknowledgment:

This research was funded by Department of Energy Grant DE-FG02-86NE37969.

## 6. REFERENCES

1. Barshan, B. and Durrant-Whyte, H.F., 1995, "Inertial Navigation Systems for Mobile Robots."

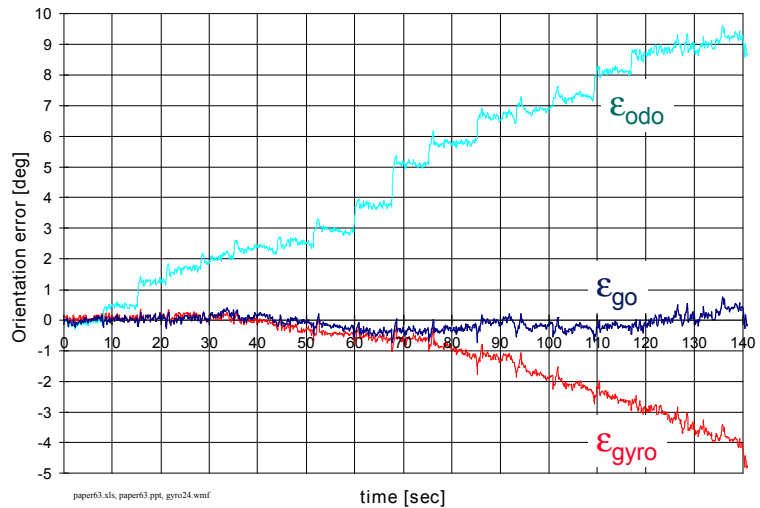


Figure 4: Same 2-minute run as in Fig. 2, but here showing orientation errors resulting from measurements based on odometry ( $\theta_{odo}$ ), the gyro ( $\theta_{gyro}$ ), and the Gyrodometry method ( $\theta_{go}$ ).

IEEE Transactions on Robotics and Automation, Vol. 11, No. 3, June 1995, pp. 328-342.

2. Borenstein, J., 1995, "Internal Correction of Dead-reckoning Errors With the Compliant Linkage Vehicle." *Journal of Robotic Systems*, Vol. 12, No. 4, April 1995, pp. 257-273.
3. Borenstein, J. and Feng, L., 1995a, "Correction of Systematic Dead-reckoning Errors in Mobile Robots." *Proceedings of the 1995 International Conference on Intelligent Robots and Systems (IROS '95)*, Pittsburgh, Pennsylvania, August 5-9, 1995, pp. 569-574.
4. Borenstein, J. and Feng, L., 1995b, "UMBmark: A Benchmark Test for Measuring Dead-reckoning Errors in Mobile Robots." *1995 SPIE Conference on Mobile Robots*, Philadelphia, October 22-26, 1995. Borenstein, J., Everett, H.R., and Feng, L., 1996, "Navigating Mobile Robots: Systems and Techniques" Publisher: AK Peters., Wellesley, MA, ISBN 1-56881-058-X, Projected Publication Date: 2/96.
5. Byrne, R.H., Kiarer, P.R., and Pletta, J.B., 1992, "Techniques for Autonomous Navigation," Sandia Report SAND92-0457, Sandia National Laboratories, Albuquerque, NM, March.
6. Chenavier, F. and Crowley, J., 1992, "Position Estimation for a Mobile Robot Using Vision and Odometry." *Proceedings of IEEE International Conference on Robotics and Automation*, Nice, France, May 12-14, pp. 2588-2593. Evans, J. M.,

- 1994, "HelpMate: An Autonomous Mobile Robot Courier for Hospitals." 1994 International Conference on Intelligent Robots and Systems (IROS '94). München, Germany, September 12-16, 1994, pp. 1695-1700.
7. Everett, H.R., 1995, "Sensors for Mobile Robots," A K Peters, Ltd., Wellesley, MA.
  8. Feng, L, Koren, Y., and Borenstein, J., 1993, "A Cross-Coupling Motion Controller for Mobile Robots." IEEE Journal of Control Systems. December, pp. 35-43.
  9. Komoriya, K. and Oyama, E., 1994, "Position Estimation of a mobile Robot Using Optical Fiber Gyroscope (OFG)." International Conference on Intelligent Robots and Systems (IROS '94). Munich, Germany, September 12-16, pp. 143-149.
  10. [GEC] Avionics, Kent, U.K.
  11. [HITACHI] - Hitachi Cable America, Inc., New York Office, 50 Main Street, 12th floor, White Plains, NY 10606.
  12. [MURATA] - Murata Erie North America, 2200 Lake Park Drive, Smyrna, GA 30080.
  13. [TRC] (Transition Research Corporation), Shelter Rock Lane, Danbury, CT, 06810-8159.